

Ro-vibronic transition intensities for triatomic molecules from the exact kinetic energy operator; electronic spectrum for the $\tilde{C} \ 1B_2 \leftarrow \tilde{X} \ 1A_1$ transition in SO_2

Emil J. Zak, and Jonathan Tennyson

Citation: [The Journal of Chemical Physics](#) **147**, 094305 (2017);

View online: <https://doi.org/10.1063/1.4986943>

View Table of Contents: <http://aip.scitation.org/toc/jcp/147/9>

Published by the American Institute of Physics

Articles you may be interested in

[A general variational approach for computing rovibrational resonances of polyatomic molecules. Application to the weakly bound \$\text{H}_2\text{He}^+\$ and \$\text{H}_2\cdot\text{CO}\$ systems](#)

The Journal of Chemical Physics **147**, 094106 (2017); 10.1063/1.5000680

[A coherent discrete variable representation method on a sphere](#)

The Journal of Chemical Physics **147**, 094101 (2017); 10.1063/1.4996891

[Perspective: Computing \(ro-\)vibrational spectra of molecules with more than four atoms](#)

The Journal of Chemical Physics **146**, 120902 (2017); 10.1063/1.4979117

[Investigation of the ozone formation reaction pathway: Comparisons of full configuration interaction quantum Monte Carlo and fixed-node diffusion Monte Carlo with contracted and uncontracted MRCI](#)

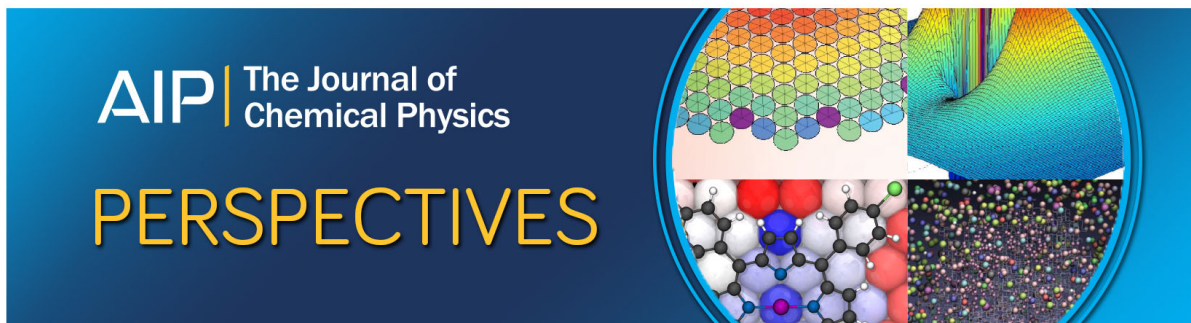
The Journal of Chemical Physics **147**, 094306 (2017); 10.1063/1.4990673

[Internal energy dependence of the photodissociation dynamics of \$\text{O}_3^-\$ using cryogenic photoelectron-photofragment coincidence spectroscopy](#)

The Journal of Chemical Physics **147**, 094307 (2017); 10.1063/1.4986500

[Cheap but accurate calculation of chemical reaction rate constants from ab initio data, via system-specific, black-box force fields](#)

The Journal of Chemical Physics **147**, 161701 (2017); 10.1063/1.4979712



Ro-vibronic transition intensities for triatomic molecules from the exact kinetic energy operator; electronic spectrum for the $\tilde{C}^1B_2 \leftarrow \tilde{X}^1A_1$ transition in SO₂

Emil J. Zak^{a)} and Jonathan Tennyson

Department of Physics and Astronomy, University College London, London WC1E 6BT, United Kingdom

(Received 7 June 2017; accepted 10 August 2017; published online 5 September 2017)

A procedure for calculating ro-vibronic transition intensities for triatomic molecules within the Born-Oppenheimer approximation is reported. Ro-vibrational energy levels and wavefunctions are obtained with the DVR3D suite, which solves the nuclear motion problem with an exact kinetic energy operator. Absolute transition intensities are calculated both with the Franck-Condon approximation and with a full transition dipole moment surface. The theoretical scheme is tested on $\tilde{C}^1B_2 \leftarrow \tilde{X}^1A_1$ ro-vibronic transitions of SO₂. *Ab initio* potential energy and dipole moment surfaces are generated for this purpose. The calculated ro-vibronic transition intensities and cross sections are compared with the available experimental and theoretical data. *Published by AIP Publishing.* [http://dx.doi.org/10.1063/1.4986943]

I. INTRODUCTION

A considerable number of triatomic species are of great importance in studies of Earth's and exoplanetary atmospheres: H₂O, CO₂, SO₂, O₃, H₂S, NO₂, HCN, etc.^{1,2} All these molecules absorb the ultraviolet (UV) light, which is associated with an electronic transition. This fact can be utilized in qualitative and quantitative characterisations of atmospheres, by comparing measured spectra to theoretical predictions. Qualitative molecular fingerprint studies with low-resolution remote-sensing instruments need only approximate band shapes and intensities provided by theory. On the other hand, quantitative analysis of concentrations of molecules from UV absorption spectroscopy requires high quality modeling of ro-vibronic line positions, line intensities, as well as line shapes.

Spectroscopic datasets such as HITRAN,³ HITEMP,⁴ and GEISA⁵ provide such line-by-line data at infrared and visible wavelengths. However at present, these databases contain no UV line-by-line data for polyatomics, although HITRAN 2016 provides cross sections for a large number of molecules including SO₂. Quantification of many compounds in Earth's atmosphere relies on the absorption of the UV radiation and line-by-line data, if available, are best for this. However, for successful retrieval of molar fractions of molecules in the atmospheric measurements, all absorption lines in a given spectral region have to be characterized, requiring high-resolution supporting data, and this currently represents a major challenge. In addition to that, reference spectra taken directly from experiment show issues with completeness of the data as well as insufficient quality of line intensities. This creates a demand for a systematic scheme for producing low

uncertainty spectroscopic parameters for ro-vibronic transitions. In the infrared absorption region, theoretical calculations with the DVR3D suite by Tennyson *et al.*⁶ were shown to provide high accuracy line intensities for molecules such as CO₂^{7–10} and H₂O.^{11–15}

The present paper proposes a theoretical procedure that can be used to generate UV absorption line positions and transition intensities for triatomic molecules. This is achieved by extending the existing DVR3D code for ro-vibrational infrared calculations onto electronic transitions in the UV. The resulting calculated parameters of ro-vibronic transitions are supposed to serve as a theoretical reference model for measured line positions and transition intensities, for further utilization in the atmospheric science.

There are a number of theoretical methods and their computer implementations for the calculation of UV absorption spectra of triatomic molecules. Transition frequencies are often directly determined from measurements or indirectly from effective Hamiltonian models,^{16–18} which give much higher accuracy than variational calculations. On the other hand, transition intensity calculations often require support from *ab initio* models.¹⁹ These models, in order to meet the high accuracy requirement, need to be derived from appropriately high level electronic structure calculations and nuclear motion theory. Resolution of rotational lines is thus necessary which means that couplings between the rotational, vibrational, and sometimes electronic motion must be considered.

Electronic transitions triggered by UV photons can be modeled quantum-mechanically from a range of perspectives. The most common approach uses empirically tuned effective Hamiltonians supported by Franck-Condon transition intensities.²⁰ Effective Hamiltonians rely heavily on the experimental data that are often of limited availability and quality. Thus, although accurate, the effective Hamiltonian approach has a drawback of limited robustness, as typically a separate

^{a)}Author to whom correspondence should be addressed: emil.j.zak@gmail.com

quantum mechanical model is needed for every molecule and every isotopologue.^{21–23} For this reason, *ab initio* methodologies for calculating ro-vibronic transition frequencies and intensities are usually employed, serving as the first stage in the modeling process.^{7–9,24} Furthermore, the *ab initio* method can be extended to consider highly excited states that are important for high temperature studies such as those needed for exoplanets. Exotic or poisonous chemical species, such as TiO, VO, PH₃, or H₂F⁺, some of which exist in the interstellar medium, are prominent examples of systems, for which *ab initio* theory is the only viable approach to prediction of infrared (IR) or UV spectra.^{25–27} Experimental characterization of this type of molecules is largely inhibited by problems with synthesis and stability of compounds, as well as temperature limitations in laboratory measurements.

A number of programs for solving the ro-vibronic Schrödinger equation are available, such as RENNER^{28–30} by Odaka *et al.*, which is dedicated to linear Renner-type triatomic molecules or more general variational codes for solving the triatomic spin-ro-vibronic problem based on MORBID by Jensen *et al.*,^{31–34} which uses an approximate kinetic energy operator for nuclei, RVIB3^{35–37} by Carter and Handy *et al.* is designed only for semi-rigid triatomic molecules with three or less interacting electronic states. A bottleneck in the variational methodology is diagonalising the large matrices required for calculations of highly excited rotational states; thus its applicability is limited by computing power. This limitation can be partially overcome with the use of the discrete variable representation (DVR),^{38–40} which is presently well-known for its computational efficiency. The DVR3D suite by Tennyson *et al.*^{6,41} uses an exact kinetic energy (EKE) operator and further optimized the solution to the ro-vibrational Schrödinger equation in a two-step procedure.⁴² The DVR3D computer code has been used to generate a considerable number of ro-vibrational line lists,^{7–9,43,44} with wavefunctions and energy levels calculated in several cases up to values of the rotational quantum number $J > 100$. The accuracy of these wavefunctions and energy levels is largely determined by the quality of the potential energy surface (PES) and the dipole moment surface (DMS). The accuracy of transition intensities in our recent ro-vibrational line lists generated with *ab initio* DMS has reached and arguably exceeded experimental accuracy.^{7–10,45} As a result, for 12 isotopologues of carbon dioxide in the 0–8000 cm⁻¹ wavenumber range, the theoretical transition intensities calculated with DVR3D were included in the HITRAN2016 spectroscopic database.³ Here, we extend the thoroughly tested DVR3D computer code to electronic excitations.

Time-dependent methods have also been used to simulate IR and UV molecular spectra. Although primarily designed for larger systems, time-dependent methods, such as multi-configuration time-dependent Hartree-Fock (MCTDH)⁴⁶ or molecular dynamics, are applicable to triatomics too.⁴⁷ The main issue with current application of MCTDH and molecular dynamics approaches is the absence of detailed modeling of $J > 0$ transitions, and that no rotation-vibration couplings are reflected in wavefunctions. The effect of Coriolis couplings is, for instance, visible in the UV spectrum of SO₂ ($\tilde{C}^1B_2 \leftarrow \tilde{X}^1A_1$ electronic transition).^{20,48} Another serious

disadvantage of MCTDH methods is the approximate Hamiltonians used, which bring a limited control over accuracy of calculations for highly anharmonic systems. For this reason, the EKE operator, with complete description of rotational motion as well as rotation-vibration couplings, remains the best option for high accuracy calculations. For example, some remote-sensing experiments rely on measurements of a single rotational line; hence after the identification stage, based on the recognition of a fingerprint for a given molecule, a quantitative study based on absolute and accurate ro-vibronic intensities is needed. Many models based on Franck-Condon calculations often provide only relative intensities of bands, calculated from overlaps of the vibrational wavefunctions, which are of limited use in quantitative spectroscopy.^{49,50}

The primary goal of the present paper is to introduce a procedure for solving the Schrödinger equation for any triatomic molecule, with two un-coupled electronic states in the Born-Oppenheimer approximation, and subsequent computation of transition intensities between the stationary states obtained. This theoretical scheme is tested on the SO₂ molecule. As a basis for extension of the computational scheme, we choose the well-established DVR3D suite, which operates with the EKE operator in the Born-Oppenheimer approximation. Here, we explore the possibility of extending DVR3D to the calculation of ro-vibronic spectra of triatomic molecules within the Born-Oppenheimer approximation and with transition dipole moment surface (TDMS) between two electronic states. DVR3D has already been successfully applied in ro-vibrational calculations of energy levels and wavefunctions in electronically excited states of FeCO.⁵¹ The next procedural step is to enable computation of transition intensities between two Born-Oppenheimer electronic states. Here, this is done at two levels of approximation: the Franck-Condon (FC) approximation⁵² with ro-vibrationally coupled wavefunctions and the transition dipole moment surface approach, which accounts for the dependence of the electronic transition dipole moment on internal coordinates of the molecule.

As a case study for the new procedure, the UV absorption spectrum for the $\tilde{C}^1B_2 \leftarrow \tilde{X}^1A_1$ electronic transition in SO₂ is calculated. Sulfur dioxide plays a substantial role in atmospheric chemistry. Detailed understanding of vibronic absorption properties of all major isotopologues of sulfur dioxide is essential for explaining the mass-independent isotope fractionation effect observed for SO₂ in Earth's atmosphere.⁵³ SO₂ is a major component of Venus' atmosphere, it also accompanies Earth's volcanic activity and industrial activities. Sources and migrations can be monitored by detecting hazes of SO₂.

The infrared absorption spectra of atmospheric sulfur dioxide are often congested with absorption bands from other molecules, especially water. For this reason, measurements of SO₂ in the UV region have gained a growing attention over the years, and a few satellite instruments are currently operating in the UV light, for example, GOME-2⁵⁴ and OMI,⁵⁵ reviewed in Ref. 56. These measurements require high accuracy spectroscopic models to support assignment of lines and to provide reference line strengths for concentration

retrieval. In addition to that, cross sections at different temperatures and pressures for several molecules need to be provided prior to the measurement, in order to retrieve accurately concentrations of the molecule of interest in the atmosphere, here SO₂. Currently, such parameters can be obtained consistently only from theoretical calculations. Thus, along with the development of experimental instrumentation and methodology, a parallel progress is needed in the accurate description and understanding of the nuclear dynamics in excited electronic states of SO₂ and other atmosphere-present compounds.

The most popular choice for the UV absorbing bands are the *A* and *B* bands of SO₂ located in the 270–400 nm wavelength region,^{57,58} for which a theoretical description has been given by Xie *et al.*⁵⁹ The strongest absorption in the UV is however attributed to the dipole allowed \tilde{C}^1B_2 state. This electronic state, chosen here as a case study, has a highly anharmonic potential energy surface with a double-well structure.⁶⁰ Although the strongest absorption for the $\tilde{C}^1B_2 \leftarrow \tilde{X}^1A_1$ transition is located near 200 nm,⁶¹ for the present purposes, we chose the longer wavelength 220–235 nm absorption region, which involves transitions to the lowest vibrational states of the \tilde{C}^1B_2 electronic state, due to limitations of the *ab initio* potential energy surface used here.

High resolution spectra for the $\tilde{C}^1B_2 \leftarrow \tilde{X}^1A_1$ electronic transition in the 220–235 nm region were recorded by Yamanouchi *et al.*,⁵⁰ Rufus *et al.*,⁶² and more recently by Blackie *et al.*,⁶³ where a review on past measurements is presented. Other lower resolution measurements were published by several authors, see, for example, the work of Danielache *et al.*⁶⁴ and Sako *et al.*⁶⁵ There are a number of theoretical studies on spectroscopy of the \tilde{C}^1B_2 state. Early papers by Xie *et al.*⁶⁶ and Bludský *et al.*⁶⁷ paved the way for more accurate descriptions, recently provided by Kłos *et al.*⁶⁸ and Kumar *et al.*⁶⁹ High quality *ab initio* spectra for the transition to the \tilde{C}^1B_2 state do not so far however include rotational structure. Results from Kłos *et al.*⁶⁸ will serve as a benchmark for $J=0$ calculations with our procedure. Particularly for non-symmetric triatomic molecules, our present approach can provide information on the so-called *axis-switching effect*,^{70–74} which is inherently accounted for in the model.

In Sec. II, general expressions for ro-vibronic line strengths in the FC and TDMS approach are derived. Section III discusses the electronic structure calculations and Sec. IV discusses the nuclear motion calculations. Results of calculations are given in Sec. V, where integral transition intensities are compared against other theoretical calculations as well as experimental data, and the significance of the TDMS is discussed.

II. METHODOLOGY

A. Ro-vibronic wavefunctions

In the new generalised version of DVR3D, transitions occur between spin-ro-vibronic states of the molecule. In the present, generic model, the total spin-ro-vibronic molecular state is assumed separable into the nuclear spin part $|\Phi^{nspin}\rangle$, the electronic part $|\Phi^{el}\rangle$, and a coupled ro-vibrational part $|\Phi^{rv}\rangle$,

$$|\Phi^{total}\rangle = |\Phi^{nspin}\rangle \otimes |\Phi^{el}\rangle \otimes |\Phi^{rv}\rangle. \quad (1)$$

Such separation means that the electronic state $|\Phi^{el}\rangle = |S, i\rangle$ is characterized by the total electronic spin quantum number *S* (spin-orbit coupling is neglected) and an index *i*, which enumerates Born-Oppenheimer electronic states. Future releases of the DVR3D code is planned to allow for mixing between electronic states. $|\Phi^{nspin}\rangle = |I, m_I\rangle$ is the nuclear spin function characterized by the total nuclear spin *I* and the projection *m_I* of the total nuclear spin vector on the space-fixed Z-axis. For a given total nuclear spin *I*, the nuclear spin wavefunctions form a finite orthonormal set and molecular energy levels associated with all nuclear spin states $|I, m_I\rangle$, $m_I = -I, -I+1, \dots, I-1, I$ are degenerate (no hyperfine interactions).⁷⁵ The total ro-vibrational state of the molecule $|\Phi^{rv}\rangle = |J, M, v, i\rangle$ is characterized by the total angular momentum *J*, the projection of the total angular momentum $M = -J, -J+1, \dots, J-1, J$ on the space-fixed Z-axis. *v* is the index enumerating ro-vibrational states. In general, the ro-vibrational part of the wavefunction also depends on the electronic state “*i*.”

In the introduced convention, the total molecular state will be denoted as

$$|N, v, i, \vec{D}\rangle = |I, m_I\rangle \otimes |S, i\rangle \otimes |J, M, v, i\rangle, \quad (2)$$

where vector \vec{D} contains all quantum numbers labelling degenerate states: *M, m_I*. Note that the ro-vibrational state in general depends on the electronic state *i*, which will be explained below. $N = J - S$ is the ro-vibronic angular momentum quantum number. Because we use here the uncoupled basis for the characterisation of ro-vibrational and electronic states, and we will be considering singlet electronic states only (*S* = 0), *J* label will be used for the ro-vibronic angular momentum further on.

Below, for explanatory purposes, we consider only triatomic symmetric XY₂ molecules for which the molecule-fixed axis system is chosen so that the x-axis bisects the Y–X–Y angle.⁷⁶ With a choice of symmetric internal coordinates, an additional symmetry label is possible: the *vibrational parity* *q* quantum number, related to the permutation symmetry of identical nuclei in XY₂.⁷⁶ Generalisation to non-symmetric molecules is straightforward.⁶ The present version of DVR3D⁶ allows for the choice of axis embeddings and internal coordinates including Jacobi and Radau coordinates.⁷⁷ Our present study is based on the use of Radau coordinates that are assumed in the derivations below. The ro-vibrational wavefunction can be expanded in a sum of products of rotational and vibrational wavefunctions

$$|J, M, v, i\rangle = \sum_{m,n,j} \sum_{k=-J}^J C_{mnjk}^{J,M,i,v} |m, n, j, i\rangle \otimes |J, M, k, i\rangle, \quad (3)$$

where summation goes over *m, n, j* which label vibrational states for stretching, stretching, bending, respectively, and *k* is the projection of the total angular momentum on the molecule-fixed z-axis. $|J, M, k, i\rangle$ is the symmetric-top Hamiltonian eigenfunction, which in general needs to be defined separately for every electronic state. Similarly the vibrational basis is defined separately for every electronic state *i*. As shown by Sutcliffe and Tennyson,⁷⁶ a very efficient definition of ro-vibrational states involves coupling of vibrational bending

states with rotational states separately from the vibrational-stretching states. For this reason, instead of the general rotation-vibration sum of products functional form given in Eq. (3), a modified basis is used,

$$\begin{aligned} |J, M, k, j, i, p\rangle = & \frac{1}{\sqrt{2(1 + \delta_{k0})}} |jk, i\rangle \otimes (|J, M, k, i\rangle^* \\ & + (-1)^{p+k} |J, M, k, i\rangle), \end{aligned} \quad (4)$$

where $|jk, i\rangle$ is a normalized bending basis state in the electronic state i , given in the position representation by the *associated Legendre polynomials*. The phase convention of Condon and Shortley⁷⁸ is used for the bending states. $|J, M, k, i\rangle$ vectors are the previously defined rotational basis states corresponding to the eigenstates of the symmetric-top Hamiltonian. The quantum number p is associated with the *parity* symmetry and determines the *elf* labels for ro-vibrational states ($p=0$ for the e state and $p=1$ for the f state); k takes integer values from p to J .

In addition to the rotation-bending coupled basis, the vibrational-stretching basis can be further symmetry-adapted by utilizing the *vibrational parity* q quantum number

$$\begin{aligned} |m, n, i, q\rangle = & \frac{1}{\sqrt{2(1 + \delta_{mn})}} (|m, i\rangle \otimes |n, i\rangle \\ & + (-1)^q |n, i\rangle \otimes |m, i\rangle), \end{aligned} \quad (5)$$

where $|m, i\rangle \otimes |n, i\rangle$ stands for the tensor product of vibrational basis states for the electronic state i associated with the first r_1 and the second r_2 stretching Radau coordinate, respectively. m and n label the 1D basis states. Vibrational parity takes two values: $q=0$ for “even” vibrational states and $q=1$ for “odd” vibrational states. Note that the character of the permutation P_{12} of identical nuclei acting on the basis state in Eq. (5) is $(-1)^{q+k}$ and the character of the parity E^* operation acting on the basis state in Eq. (4) is $(-1)^{p+J}$.

Utilization of the rotational parity and the vibrational parity decomposes the *Hilbert space* of the problem into simple sum of four independent sub-spaces for each J and i values: $\mathcal{H}_{p,q}^{J,i} \oplus \mathcal{H}_{p,1-q}^{J,i} \oplus \mathcal{H}_{1-p,q}^{J,i} \oplus \mathcal{H}_{1-p,1-q}^{J,i}$. The electronic dipole moment operator $\hat{\mu}_{el}$ mixes these subspaces according to rigorous selection rules: $|\Delta q|=1$ and for $\Delta J=0$: $|\Delta p|=1$ and $\Delta J=\pm 1$: $|\Delta p|=0$.

To summarize, the final ro-vibronic basis set used in the present implementation of DVR3D is given by the expression

$$\begin{aligned} |J, M, v, i, p, q\rangle = & \sum_{m,n,j} \sum_{k=p}^J C_{mnjk}^{J,M,i,v,p,q} |m, n, i, q\rangle \\ & \otimes |J, M, k, j, i, p\rangle. \end{aligned} \quad (6)$$

A two-step procedure^{78–80} of solving the nuclear Schrödinger equation in the basis defined by Eqs. (5) and (4) is applied. This is the key to efficient solution for problems with high J . The first step involves solving the Coriolis-decoupled ro-vibrational motion problem for every combination of the (J, l, k, i) quantum numbers separately. A complete rotational basis set is used, meaning that $k=p, p+1, \dots, J$ and $p=0, 1$. The integrated over rotational degrees of freedom effective Hamiltonian for the first step of calculation can be written as

$$\hat{H}_{k,i} = \hat{K}_v + \delta_{k,k'} \hat{K}_{rv} + V_i, \quad (7)$$

where \hat{K}_v is the vibrational part of an exact kinetic energy operator and $\delta_{k,k'} \hat{K}_{rv}$ is the diagonal part of the exact effective kinetic energy operator produced by rotational integration of the ro-vibrational part of the total EKE operator. V_i is the i -th electronic state potential energy function of nuclei generated from electronic structure calculations. Solutions to the first step, in which k is a good quantum number, supply a basis for the second step, where the full ro-vibrational Hamiltonian is considered, with a non-diagonal ro-vibrational Hamiltonian. The excellent basis from the first stage ensures very fast convergence of solutions in the second stage. In addition to this, matrix elements of the Hamiltonian are represented on a previously optimized discrete variable representation (DVR) grid. In DVR3D, the stretching degrees of freedom are modeled with the spherical-oscillator basis set of a Morse-like oscillator basis set, which in DVR corresponded to Gauss-Laguerre quadratures. For bending motion, the *associated Legendre polynomials* are used, which in DVR correspond to a Gauss-Legendre quadrature scheme. The choice of *associated Legendre polynomials* has also another motivation: it eliminates singularity⁷⁶ at linear geometries from the Hamiltonian in Eq. (7). By definition, the number of chosen vibrational basis states is equal to the number of DVR integration points. The solution strategy described above has been proven very successful in accurate calculations of energy levels with high values of J quantum number.^{7–9,43,44}

B. Axis-switching effect

Not only does the equilibrium geometry of the molecule change upon the electronic transition but also an additional rotation of the molecule-fixed coordinate system is required.⁷⁰ The former effect can be directly attributed to the difference in shapes of the potential energy surfaces for the two electronic states that cause the vibrational basis set optimized for the electronic excited state to be no longer optimal for the electronic ground state. In the terminology of normal modes, it means that normal coordinates in the electronic excited states are rotated (leading to the so-called Duschinsky effect^{72,73,81}) with respect to normal coordinates in the electronic ground. The effect of rotation of the molecule-fixed coordinate system affects the Euler angles, causing rotation of the rotational basis set. Although in many systems these artifacts of the electronic transition are marginal, they sometimes significantly soften rotational selection rules, allowing for the appearance of whole vibrational bands forbidden, as observed in HCN⁷¹ and SiHD.⁷⁴ For example, in the HCN molecule, for the $(\pi^* \leftarrow \pi)$ electronic transition, only $\Delta K=\pm 1$ sub-bands are allowed by rotational selection rules. However stimulated-emission-pumping (SEP) experiments⁸² observed weak $\Delta K=0$ transitions to levels with non-zero vibrational angular momentum ($l=1$). This type of transition is forbidden by rotational selection rules and has been convincingly attributed to non-rigidity of the molecule during the transition between linear \tilde{X} electronic ground state and bent \tilde{A} electronic state.^{70,71} In calculations, the magnitude of the axis-switching effect depends on the choice of the molecule-fixed frame and the choice of coordinates and the basis set. Axis-switching is strongly

pronounced in the *Eckart frame*, the molecule-fixed coordinate system which needs to be rotated when changing the electronic state, in order to satisfy the conditions of the minimal rotational-vibrational coupling in both states separately.

The axis-switching effect tells us that the rotational basis functions should be labelled with the quantum numbers for electronic states too. However, the completeness of the rotational basis used in the present model guarantees that the rotational part is accounted for exactly regardless of the electronic states. Therefore, rotational states in the electronic excited state, which are nominal functions of rotated Euler angles can be modeled with the un-rotated rotational basis of the electronic ground state (or vice-versa). An appropriately large vibrational basis set can also eliminate any inaccuracies resulting from the *Duschinsky effect*, meaning that the vibrational basis is nearly complete hence does not depend on the electronic state. For the reasons discussed above, we can drop the electronic index i for the rotational and vibrational basis states in Eqs. (4) and (5). Thus, at the cost of extra computational time, the geometric effects associated with the electronic transition are almost entirely eliminated. Thus, ro-vibronic transitions forbidden by rotational selection rules, which appear in line lists calculated with our model, may be attributed to the axis-switching effect.

Our approach utilizes an identical basis set to calculate ro-vibrational energies and wavefunctions in the ground and the excited state of the molecule (we assume a system with two electronic states). In DVR, this means that the ro-vibrational wavefunctions for both electronic states are defined on the same grid, which provides the advantage of straightforward integration over internal coordinates of the molecule. For this reason, matrix elements between ro-vibrational states of the electronic ground and excited states can be evaluated as a sum of products of respective functions at given grid points.

C. Transition intensities

Quantum probability for the $|v''\rangle \equiv |J'', v'', i'', p'', q'', \vec{D}''\rangle \rightarrow |v'\rangle \equiv |J', v', i', p', q', \vec{D}'\rangle$ ro-vibronic transition is given in the dipole approximation by the square modulus of the electric transition dipole moment vector $\sum_{A=X,Y,Z} |T_{v''v'}^{A,\vec{D}'',\vec{D}'}|^2$, where the summation is carried out over three Cartesian components of the electric dipole moment of the molecule in the laboratory frame $A=X, Y, Z$. Individual transition probabilities are then summed over all degenerate states, labelled by vector \vec{D} ,

$$S_{v''v'} = \sum_{A=X,Y,Z} \sum_{\vec{D}'',\vec{D}'} |T_{v''v'}^{A,\vec{D}'',\vec{D}'}|^2, \quad (8)$$

giving a quantity called the *line strength*, which can be directly related to experimentally measured integral line intensity,

$$I(\tilde{v}_{v''v'}) = \frac{8\pi^2 N_A}{12\epsilon_0 hc} \frac{\tilde{v}_{v''v'}}{Q(T)} \exp\left(\frac{-E_i}{k_b T}\right) \left[1 - \exp\left(-\frac{\tilde{v}_{v''v'}}{k_b T}\right)\right] S_{v''v'}, \quad (9)$$

where $\tilde{v}_{v''v'}$ is the transition wavenumber between the v'' th and v' th ro-vibronic state and $Q(T)$ is the partition function at temperature T . N_A is the Avogadro number, k_b is the Boltzmann constant, h is the Planck constant, c is the speed of light in

vacuum, and ϵ_0 is the permittivity of vacuum. Units for integral line intensity are cm/molecule.

The electric transition dipole moment is defined as

$$T_{v''v'}^{A,\vec{D}'',\vec{D}'} = \langle J'', v'', i'', p'', q'', \vec{D}'' | \hat{\mu}_{el}^{A,space} | J', v', i', p', q', \vec{D}' \rangle$$

and its value is identical for all components of \vec{D} , hence this index can be dropped from the expression. The space-fixed transition dipole moment can be transformed into a *spherical tensor form*, which transforms irreducibly in the 3D rotations group

$$\vec{\mu}_{el,sph}^{space} = \mathbf{K} \vec{\mu}_{el}^{space}, \quad (10)$$

where

$$\mathbf{K} = \begin{pmatrix} -\frac{1}{\sqrt{2}} & \frac{i}{\sqrt{2}} & 0 \\ \frac{1}{\sqrt{2}} & \frac{i}{\sqrt{2}} & 0 \\ 0 & 0 & 1 \end{pmatrix} \quad (11)$$

is a unitary ($|\det(\mathbf{K})| = 1$, $\mathbf{K}^\dagger \mathbf{K} = \mathbf{1}$) transformation matrix between the Cartesian operator and *rank 1 spherical tensor operator*. Dipole moment for a neutral molecule is invariant under translations in free space, the 'LAB' components (X, Y, Z) of the transition dipole moments can be rewritten in terms of Cartesian components in the space-fixed coordinate system (ξ, η, ζ) with the origin at the nuclear center of mass.⁷⁵ What follows, the transition dipole moment may be expressed as

$$T_{v''v'}^A = \sum_{A=\xi,\eta,\zeta} \sum_{\sigma=-1}^1 \mathbf{K}_{A\sigma}^\dagger \sum_{\vec{D},\vec{D}'} \tilde{T}_{v''v'}^{\sigma,M,M'}. \quad (12)$$

As a result of new transformation properties of the transition dipole vector, a straightforward transformation to the molecule-fixed coordinate system can be achieved with Wigner D-matrices

$$\vec{\mu}_\sigma^{space} = \sum_{\sigma'=-1}^1 \mathbf{D}_{\sigma\sigma'}^{(1)}(\phi, \theta, \chi) \vec{\mu}_{\sigma'}^{mol}, \quad (13)$$

where ϕ, θ, χ denote Euler angles and subscripts "el" and "sph" have been dropped for clarity of presentation. After rather lengthy algebra with extensive use of properties of 3-j symbols, the line strength takes the form

$$\begin{aligned} S_{v''v'} = & \frac{1}{4} g_{ns} (2S'' + 1) (2S' + 1) (2J'' + 1) \\ & \times (2J' + 1) [(-1)^{J''+J'+1} + (-1)^{p''+p'}]^2 \\ & \times \left| \sum_{\sigma=-1}^{+1} \sum_{\substack{j',j'' \\ k'=p' \\ k''=p''}}^{+1} (-1)^{k''} b_{q'q''}^\sigma \begin{pmatrix} 1 & j' & j'' \\ \sigma & k' & k'' \end{pmatrix} \right. \\ & \times \left. \sum_{\substack{m',n',j', \\ m'',n'',j''}} C_{m'n'j'k'}^{j',i',v',p',q'} C_{m''n''j''k''}^{j'',i'',v'',p'',q''} M_{m'm''n'n''j'j''k'k''}^{\sigma,i'',i'} \right|^2. \end{aligned} \quad (14)$$

The $(2S' + 1)(2S'' + 1)$ prefactor in Eq. (14) comes from summation over all combinations of degenerate electron spin functions. As the electronic spin is preserved in a transition within

the present model, $S'' = S'$. Similarly, the $(2J' + 1)(2J'' + 1)$ prefactor comes from summation over all combinations of degenerate rotational basis functions, characterized by the M quantum number. g_{ns} is the spin statistical weight for the initial state i result from summation over degenerate nuclear spin functions. The values of spin statistical weights depend on the ro-vibronic symmetry of the state. $b_{q'q''}$ is a symmetry dependent numerical factor defined in Ref. 6. $M_{m'm''n'n''j'j''k'k''}^{\sigma,i'',i'}$ is the matrix element of the electric dipole moment operator in the primitive vibrational basis,

$$M_{m'm''n'n''j'j''k'k''}^{\sigma,i'',i'} = \langle j''k'' | \langle m'' | \langle n'' | \times \mu_{\sigma}^{i'',i'}(r_1, r_2, \theta) | n' \rangle | m' \rangle | j'k' \rangle, \quad (15)$$

where

$$\mu_{\sigma}^{i'',i'}(r_1, r_2, \theta) = \langle \Phi_{i''}^{el} | \hat{\mu}_{\sigma}^{mol} | \Phi_{i'}^{el} \rangle \quad (16)$$

is the σ -th spherical tensor component of the molecule-fixed electronic transition dipole moment surface between electronic states i'' and i' . In Eq. (16), integration is carried over electronic coordinates only, leaving dependence on three internal (Radau) coordinates r_1, r_2, θ . This function is called the *electronic transition dipole moment surface* (TDMS). For many molecules, the dependence of TDMS on internal coordinates is weak, and it is often replaced by a constant value of the transition dipole at equilibrium geometry $\mu_{\sigma}^{eq} \equiv \mu_{\sigma}^{ge}(r_1^{eq}, r_2^{eq}, \theta^{eq})$. In such a case, we talk about the *Condon approximation* to the electronic transition dipole moment

$$M_{m'm''n'n''j'j''k'k''}^{\sigma,i'',i'} = \mu_{\sigma}^{i'',i'}(r_1^{eq}, r_2^{eq}, \theta^{eq}) \langle m'' | m' \rangle \times \langle n'' | n' \rangle \langle j''k'' | j'k' \rangle \quad (17)$$

due to the choice of the identical orthonormal basis in the ground and the excited electronic states, the integrals in Eq. (17) become Kronecker's deltas

$$M_{m'm''n'n''j'j''k'k''}^{\sigma,i'',i'} = \mu_{\sigma}^{i'',i'}(r_1^{eq}, r_2^{eq}, \theta^{eq}) \delta_{m'm'} \delta_{n'n''} \delta_{j''j'}, \quad (18)$$

which significantly reduces the number of summed terms in the expression for the line strength so that only the elements with the same indices in the coefficients vectors $C_{m'n'j'k'}^{J'',M'',i'',v'',p'',q''}$ are needed. This simplification compensates the extra computational time needed for wavefunction calculations when using identical grid for all electronic states,

$$S_{v''v'} = \frac{1}{4} g_{ns} (2S'' + 1)^2 (2J'' + 1) \times (2J' + 1) [(-1)^{J''+J'+1} + (-1)^{p''+p'}]^2 \times \left| \sum_{\sigma=-1}^{+1} \mu_{\sigma}^{eq} \sum_{\substack{k'=p' \\ k''=p''}}^{J',J''} (-1)^{k''} b_{q'q''}^{\sigma} \begin{pmatrix} 1 & J' & J'' \\ \sigma & k' & k'' \end{pmatrix} \times \sum_{m'',n''j''} C_{m'n'j'k'}^{J',i',v',p',q'} C_{m''n''j''k''}^{J'',i'',v'',p'',q''} \right|^2. \quad (19)$$

The 3-j symbol appearing in Eqs. (14) and (19) and the $[(-1)^{J''+J'+1} + (-1)^{p''+p'}]^2$ factor are responsible for selection rules. From the former, it follows that in order for the line strength not to vanish, the following conditions must be

satisfied: $|J'' - J'| = 0, 1, J'' + J' \geq 1$, and $\Delta|k| = 0, \pm 1$. Selection rules for the J quantum number define P, Q, R branches for $\Delta J = J'' - J' = +1, 0, -1$, respectively. Selection rules for the k quantum number allow transitions of type $k \rightarrow -k$, which reflects time-reversal symmetry of the system. For $\Delta k = 0$, only the z -component of the molecule-fixed electronic transition dipole moment contributes to the overall line intensity, and because z -axis is chosen here as the axis of quantization, we call these transitions *parallel*. Accordingly $\Delta k = \pm 1$ corresponds to *perpendicular* transitions, as both x components of the electronic transition dipole moment contribute to the total intensity. For the Q branch ($\Delta J = 0$), only transitions which change the p quantum number are allowed, i.e., $e \leftrightarrow f, e \leftrightarrow e, f \leftrightarrow f$. Conversely, P and R branches allow transitions conserving p , i.e., $e \leftrightarrow f, e \leftrightarrow e, f \leftrightarrow f$. Neglecting the dependence of the TDMS on nuclear coordinates does not affect the rotational selection rules, it can however make the vibrational selection rules stronger, for example, by forbidding vibrational overtone transitions.

The DIPOLE3 code, which we use for the calculation of intensities in the present work, uses a DVR representation for ro-vibrational wavefunctions, which are related to the finite basis representation by an unitary composite transformation⁶

$$C_{m''n''j''k''}^{J'',i'',v'',p'',q''} = \sum_{\alpha,\beta,\gamma} (T)_{j\gamma}^{k''=0} (T)_{m\alpha} (T)_{n\beta} C_{\alpha\beta\gamma k''}^{J'',i'',v'',p'',q''}, \quad (20)$$

where the unitary transformation matrix for the bending coordinate $(T)_{j\gamma}^{k''=0}$ is defined on a Gauss-Legendre quadrature grid for $k=0$ and the unitary transformation matrices for stretching coordinates $(T)_{m\alpha}$ and $(T)_{n\beta}$ are defined over the Gauss-Laguerre quadrature grid.

III. POTENTIAL ENERGY AND TRANSITION DIPOLE MOMENT SURFACES

The potential energy surface for the \tilde{C}^1B_2 electronic state was generated from 3000 geometries in bond length–bond angle coordinates. Stretching coordinates were chosen in the range: $r_1, r_2 \in [1.2; 1.9] \text{ \AA}$, with 0.05 Å increment. Angles between the S–O bonds were sampled from 60° to 180° with 5° increments.

Electronic structure calculations were performed with the explicitly correlated multi-reference internally contracted configuration interaction method with Davidson correction (ic-MRCI-F12 + Q) in the aug-cc-pVTZ basis set, as implemented in the MOLPRO2015 package.⁸³ The reference wavefunctions were calculated with the state-averaged CASSCF method, with equal weight averaging over two singlet states. For 18 electrons occupying 19 orbitals, 12 orbitals were used ($9a'$, $3a'$) for the active space and 7 as core orbitals ($6a'$, $1a''$). The PES was fitted with the least-squares method to the functional form

$$V(y_1, y_2, y_3) = \sum_{j,k,l} C_{jkl} y_1^j y_2^k y_3^l, \quad (21)$$

where $y_1 = \frac{1}{2}(x_1 + x_2)$, $y_2 = \frac{1}{2}(x_1 - x_2)$, and $y_3 = \theta - \theta_{eq}$. Here x_1, x_2 are the Morse coordinates $x_1 = 1 - e^{-a_1(r_1 - r_1^{eq})}$ and $x_2 = 1 - e^{-a_2(r_2 - r_2^{eq})}$. The functional form and coefficient were

chosen to secure the correct shape of the PES at C_{2v} geometries. For a fixed angle $\theta = \theta_0$, the PES $V(r_1, r_2, \theta_0)$ has a saddle point when $r_1 = r_2$, and two non- C_{2v} minima in the r_1-r_2 plane, which are symmetry connected, as shown in Fig. 1. A non-uniformly weighted fit to 623 *ab initio* points with energies below 5000 cm^{-1} in $\theta \in [90^\circ; 130^\circ]$ gave $\sigma = 12 \text{ cm}^{-1}$ root-mean square residual (rmsr) between the fitted surface and *ab initio* points.

The global C_s equilibrium geometry for \tilde{C}^1B_2 is located at $r_1^{eq} = 1.640 \text{ \AA}$, $r_2^{eq} = 1.496 \text{ \AA}$, and $\theta^{eq} = 104.3^\circ$. There are two other local minima near $\theta = 80^\circ$ and $\theta = 165^\circ$. The latter is a C_{2v} symmetric minimum with energy 400 cm^{-1} above the global minimum. This well, displayed in Fig. 8, generates additional low lying energy levels that have not yet been characterized by infrared absorption spectroscopy. A separate fit for the second well near linearity gave rmsr = 17 cm^{-1} .

For the electronic \tilde{X}^1A_1 state, we used a highly accurate potential energy surface of Huang *et al.*^{84,85} This is a semi-empirical PES based on CCSD(T)/cc-pVQZ-DK calculations and refinement to experimental energy levels in the $J = 0-80$ range. The rmsr of the fit to *ab initio* points was 0.21 cm^{-1} below $30\,000 \text{ cm}^{-1}$ and the root-mean square deviation from experimental levels was 0.013 cm^{-1} . The equilibrium geometry of the electronic ground state $r_1^{eq} = 1.431 \text{ \AA}$, $r_2^{eq} = 1.431 \text{ \AA}$ and $\theta^{eq} = 119.32^\circ$ corresponds to C_{2v} symmetry.

The transition dipole moment surface between \tilde{X}^1A_1 and \tilde{C}^1B_2 electronic states was calculated as the expectation value of the electric dipole moment operator, at the same level of theory as the \tilde{C}^1B_2 PES. A fit to the functional form from Eq. (21) was performed with 1852 *ab initio* points in the $[85^\circ; 140^\circ]$ angle range. The rmsr for the x-component of the surface (x-axis chosen to bisect the angle between S–O bonds) was 0.03 a.u., and the rmsr for the z-component of the surface was 0.02 a.u. High accuracy is not the aim of the present paper, thus these values for residuals were acceptable. At equilibrium geometry, the z-component of the transition dipole moment vanishes, as shown in Fig. 2. The transition dipole moment depends on the nuclear coordinates relatively weakly, nevertheless the non-constant TDMS may

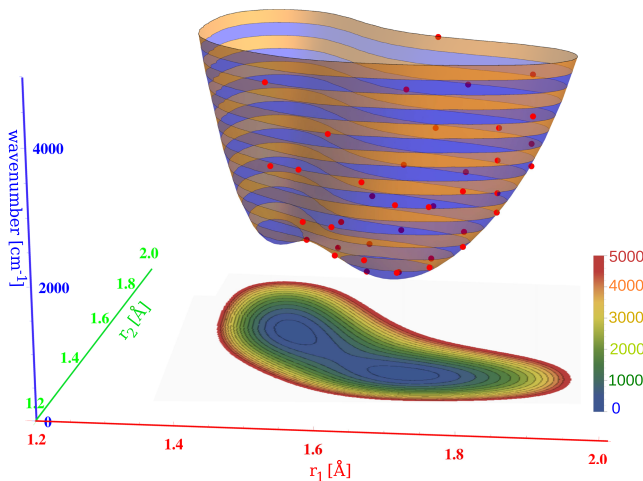


FIG. 1. Potential energy surface for the \tilde{C}^1B_2 electronic state calculated at $\theta = 120.0^\circ$. *Ab initio* points are marked in red.

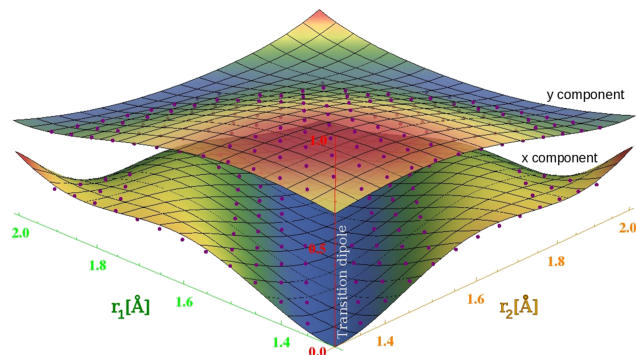


FIG. 2. Two components of the transition dipole moment function between \tilde{X}^1A_1 and \tilde{C}^1B_2 electronic states for $\theta = 120.0^\circ$. The upper surface is the y-component and the lower surface is the x-component, which vanishes for C_{2v} geometries. *Ab initio* points are marked with red.

significantly influence transition intensities; this is discussed in Sec. V.

Both the \tilde{C}^1B_2 PES and TDMS are available in the [supplementary material](#) in the form of Fortran95 routines.

IV. NUCLEAR MOTION CALCULATIONS

Born-Oppenheimer ro-vibrational wavefunctions and energy levels were obtained separately for the \tilde{X}^1A_1 and the \tilde{C}^1B_2 electronic states. For each electronic state, a two-step procedure described in Sec. II of solving the nuclear Schrödinger equation was applied. The DVR representation of matrix elements of the Hamiltonian, as implemented in DVR3D, carries the advantage of a diagonal potential energy matrix in any chosen basis. A Morse-like oscillator basis set^{6,86} was used for the S–O stretching coordinates and associated Legendre functions for the bending motion. The parameters of the stretching basis set were optimized to ensure the fastest convergence of $J=0$ energy levels in the \tilde{C}^1B_2 electronic state. The vibrational energy levels are insensitive to the value of the dissociation energy D_e in the Morse-like oscillator basis functions, hence D_e was set to 0.3 a.u. in all cases. The equilibrium bond length r_e and width α of the Morse-like basis were scanned in the $r_e \in [2.8; 3.5]a_0$ and $\alpha \in [0.008; 0.030]E_h$ regions for different sizes of the stretching basis (the NPNT parameter in DVR3D in the 30–90 range). The number of angular basis functions was independently optimized, and the corresponding NALF parameter was set to 60. As a result, the optimal set of basis set parameters was: $r_e = 2.9 \text{ } a_0$, $D_e = 0.30 \text{ } E_h$, $\alpha = 0.012 \text{ } E_h$, and NPNT = 90. With this basis optimal basis set, the accuracy of vibrational energy levels in the electronic ground state was controlled by comparison with the ExoAmes line list.⁴⁴ In light of the main idea of the present paper, we do not require spectroscopic accuracy for present calculations. For this reason, we established convergence criteria at 2 cm^{-1} and tolerance for deviation from the experiment at 20 cm^{-1} for the lowest $J=0$ energy level of the \tilde{C}^1B_2 electronic state.

The final size of the Hamiltonian was truncated at 1000, which was sufficient to provide good convergence for the lowest 100 energy levels. Diagonalisation of this matrix leads to ro-vibrational energy levels and wavefunctions labelled by the J -rotational quantum number and the e/f-Wang symmetries.

Nuclear masses in Dalton units (Da) for sulfur and oxygen were used: 31.963 294 Da (^{32}S) and 15.990 525 Da (^{16}O).⁸⁷ For the evaluation of integrals, 90-point Gauss-Laguerre and 60-point Gauss-Legendre quadratures were used, for stretching and bending coordinates, respectively. With this choice, the range of quadrature points for stretching coordinates is $r_i \in [1.13; 1.86] \text{ \AA}$; thus, this range is contained in the domain of applicability of the present fit. With this basis set, the zero-point energies for the $\tilde{\chi}^1\text{A}_1$ and $\tilde{C}^1\text{B}_2$ electronic states are $\text{ZPE}_g = 1538.19 \text{ cm}^{-1}$ and $\text{ZPE}_e = 776.45 \text{ cm}^{-1}$, respectively. In the second variational step (program ROTLEV3), for each J value, 200 ro-vibrational basis functions were separately used to solve the full Coriolis-coupled nuclear motion problem.

Identical embeddings, coordinates, and DVR grids were chosen for both electronic states. The criterion for this choice was to optimize the accuracy of the electronic excited state. The simple shape of the ground state PES gives weaker dependence on the choice of embedding and basis set parameters, when appropriately large basis set is used. Radau internal coordinates were chosen for the description of vibrational degrees of freedom. The z-axis of the molecule-fixed frame was chosen along one of the Radau coordinates (r_1), which nearly overlaps with one of the S–O bonds (“bond embedding”). The bond embedding was observed to give a significantly better convergence than the bisector embedding for the $\tilde{C}^1\text{B}_2$ electronic state, which has its equilibrium geometry at two non-equivalent S–O bond lengths, that is at C_s symmetry. The fit of the PES for the $\tilde{C}^1\text{B}_2$ state necessitated adding walls at large internuclear distances to avoid potential dropping to non-physical values. The positions of these walls were adjusted so as not to influence the values of energy levels for the present basis size. For larger basis sizes, the range of quadrature points for stretching coordinates can sample regions of the fitted PES, which are beyond the range of applicability of the present fit. These regions have high energy, thus adding walls with energy $0.1E_h$ to the present fit assures the correct asymptotics for all r_1 and r_2 values. The potential walls were added at $r=1.3 \text{ \AA}$, $r=2.0 \text{ \AA}$ and $\theta=85^\circ$, $\theta=130^\circ$.

V. RESULTS AND DISCUSSION

$J=0$ energy levels calculated with the present *ab initio* PES for the $\tilde{C}^1\text{B}_2$ electronic state are listed in Table I, where a comparison with literature calculations based on two different *ab initio* surfaces is made. The *ab initio* MRCI+Q/aug-cc-pVTZ PES by Tokue *et al.*⁸⁸ was based on 6300 geometries and was interpolated by the moving least-squares method combined with the Shepard method.⁸⁹ The *ab initio* ic-MRCI-F12+Q/aug-cc-pVTZ PES of Kłos *et al.*⁶⁸ was interpolated with spline functions. Table I also gives the semi-empirical energy levels from Jiang *et al.*²⁰ and measured energies of Yamanouchi *et al.*⁵⁰ The present calculated values for vibrational energy levels are in a good agreement with experiment and semi-empirical calculations by Jiang *et al.*²⁰ Clearly the present PES is more accurate than the one given by Tokue *et al.*⁸⁸ The root-mean square deviation (RMSD) between the experimentally tuned energy levels from Jiang *et al.*²⁰ and

TABLE I. Comparison of the $J=0$ energy levels (cm^{-1}) calculated with the present *ab initio* PES for the $\tilde{C}^1\text{B}_2$ electronic state to theoretical values from Kłos *et al.*,⁶⁸ Tokue *et al.*,⁸⁸ semi-empirical calculations by Jiang *et al.*²⁰ and measured energies.⁵⁰ In the first column, a vibrational assignment is given; the second column gives the symmetry of the state in the C_{2v} group. The b_2 levels are dipole forbidden from the vibrational ground state of the $\tilde{\chi}^1\text{A}_1$ electronic state. Energy levels from the second potential well localized around $\theta=165^\circ$ were excluded from the table.

($v_1 v_2 v_3$)	Sym.	Present	Kłos <i>et al.</i> ⁶⁸	Tokue <i>et al.</i> ⁸⁸	Jiang <i>et al.</i> ²⁰	Expt. ⁵⁰
(001)	b_2	195	223		212	
(010)	a_1	368	375	394	377	377
(002)	a_1	544	575	598	561	561
(011)	b_2	560	590		582	
(020)	a_1	734	748	772	751	752
(003)	b_2	880	912		890	
(012)	a_1	916	943	979	929	
(021)	b_2	924	956		949	
(100)	a_1	960	960	935	960	960
(030)	a_1	1101	1118		1122	1122
(004)	a_1	1246	1264		1245	1245
(013)	b_2	1258	1271		1252	
(101)	b_2	1258	1275		1261	
(022)	a_1	1289	1309		1299	1300
(031)	b_2	1291			1313	
(110)	a_1	1330			1337	1337
(005)	b_2	1465			1595	
(014)	a_1	1609			1604	1604
(023)	b_2	1631			1611	
(102)	a_1	1641			1653	1654
(032)	a_1	1647			1662	

the present calculation for $J=0$ energy levels is 13 cm^{-1} below 1500 cm^{-1} which practically equals the RMSD for the *ab initio* calculations by Kłos *et al.* The level of the present PES is comparable to the PES of Kłos *et al.*,⁶⁸ as both surfaces were calculated with the same *ab initio* method. The advantage of the present approach, which is based on a fit to a functional form, manifests in savings in the number of *ab initio* points necessary. This way of producing a PES would be thus recommended when a higher level of theory is used for the electronic structure calculations.

Analysis of Table I suggests that the present *ab initio* PES for the $\tilde{C}^1\text{B}_2$ state is applicable in the 0–1700 cm^{-1} range above the zero-point vibrational energy. This range covers vibrational energy levels involved in strong vibronic progressions thus is sufficient for comparisons to experimental room temperature electronic spectra below the dissociation threshold ($\approx 3000 \text{ cm}^{-1}$) of the $\tilde{C}^1\text{B}_2$ state. To conclude, the present PES is the most accurate *ab initio* potential energy surface for the $\tilde{C}^1\text{B}_2$ state in SO_2 , which has been fitted to a predefined functional form. A previous fit to *ab initio* points performed below 5000 cm^{-1} by Bludský *et al.*⁶⁷ gave 55 cm^{-1} rmsd with respect to measurement.

Note that at room temperature (296 K), only the lowest vibrational states of the electronic ground states are populated. Population of the asymmetric stretching fundamental $\tilde{\chi}^1\text{A}_1(0, 0, v_3)$ ($\approx 1362 \text{ cm}^{-1}$) is barely 0.1% at that temperature. Therefore in practical calculations, the number of vibrational states needed for the $\tilde{\chi}^1\text{A}_1$ electronic state is

limited to the lowest few. The variational methodology means that these lowest energy levels are calculated more accurately than higher lying states. For this reason, if the PES is accurate, as the Ames-1 PES is, satisfactory convergence can be easily achieved, even with a non-optimized basis set.

With the common basis set used in nuclear motion calculations for both electronic states, the DVR3D calculated vibrational zero-point energies for the \tilde{X}^1A_1 and \tilde{C}^1B_2 states are $ZPE_g = 1538.19 \text{ cm}^{-1}$ and $ZPE_e = 776.45 \text{ cm}^{-1}$, respectively. The former value is consistent with the 1535.63 cm^{-1} ZPE reported by Huang *et al.* and the latter value is somewhat lower than 785.75 cm^{-1} calculated by Kłos *et al.* The vertical excitation energy for the $\tilde{C}^1B_2 \leftarrow \tilde{X}^1A_1$ transition was taken from the experiment:²⁰ $T_e = 42\,573 \text{ cm}^{-1}$. Partition function at 296 K used for intensity calculations was taken from Huang *et al.*⁸⁴ [$Q(296) = 6336.789$]. The temperature range for which calculated vibronic spectra are reliable is determined by the accuracy of the ground state PES. Here, the Ames-1 PES, as very accurate, provides an opportunity for accurate modeling of vibronic hot bands. Room temperature spectra are certainly within the applicability range of the Ames-1 PES.

A. Vibronic spectra

Ab initio vibronic spectra were calculated using Eq. (9) for two cases: the Franck-Condon approximation [Eq. (18)] and with the use of the transition dipole moment surface [Eq. (14)]. The resulting transition intensities are compared in Fig. 3.

Figure 3 shows no significant alteration in strong transition intensities when the FC spectrum is compared with the TDMS spectrum. In general, for strong transitions, which contribute to the overall shape of the absorption band, the difference in the transition intensity between the FC and TDMS approach is usually less than 10%, typically 4%–6%. However, as displayed in the lower panel in Fig. 3, allowing for the dependence of the electronic transition dipole moment on nuclear coordinates can noticeably increase certain transition intensities, which are nominally very weak in the FC approximation.

Transitions from the a_1 symmetry states in the electronic ground state to the b_2 states in the electronic excited state are forbidden by vibrational dipole selection rules. However rotation-vibration interactions, especially c-axis Coriolis-type interactions, can mix states of different vibrational symmetries. The ro-vibrational selection rules require only that the irreducible representations of ro-vibrational states are identical: $\Gamma_{rv} = \Gamma'_{rv}$, where $\Gamma_{rv} = \Gamma_{vib} \otimes \Gamma_{rot}$. In the C_2v group, vibrational and rotational selection rules for the $\tilde{X}^1A_1 \rightarrow \tilde{C}^1B_2$ electronic transition allow for transitions $(a_1, eo)_{B_2} \leftarrow (a_1, ee)_{A_1}$ or $(a_1, oe)_{B_2} \leftarrow (a_1, oo)_{A_1}$ in the notation where k_a , k_b (even) is denoted as ee and k_a , k_b (odd) is denoted as oo . Ro-vibrational selection rules, which apply when states are vibrationally forbidden but are mixed by Coriolis interactions, give the following ro-vibrationally allowed transitions from a_1 states: $(b_2, oo)_{B_2} \leftarrow (a_1, ee)_{A_1}$ or $(b_2, ee)_{B_2} \leftarrow (a_1, oo)_{A_1}$.

Indeed, such transitions forbidden by vibrational selection rules but allowed by ro-vibrational selection rules have been

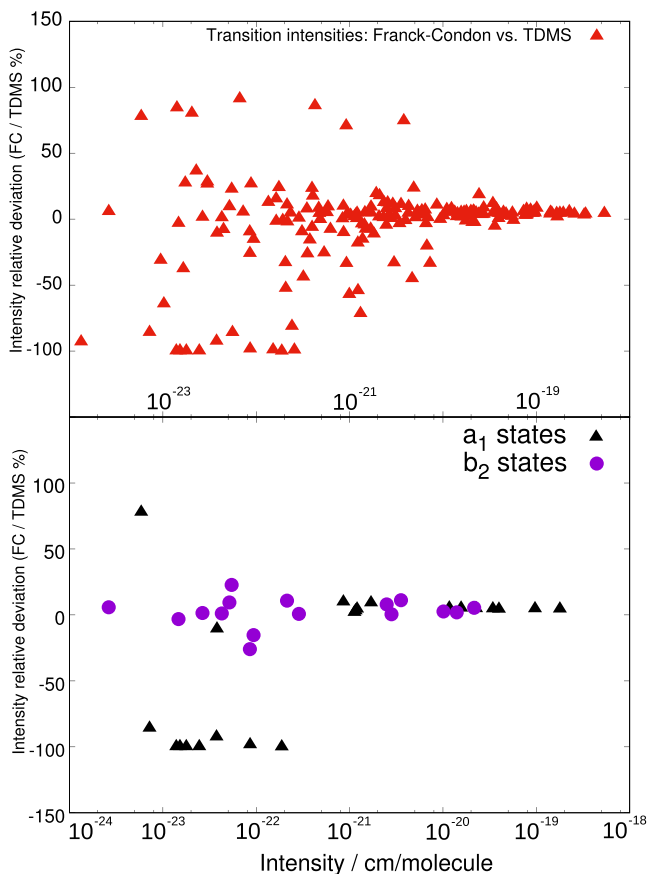


FIG. 3. Comparison of *ab initio* calculated transition intensities for the $\tilde{C}^1B_2 \leftarrow \tilde{X}^1A_1 (\nu=0)$ electronic transition ($J'=1 \leftarrow J''=0$) between the Franck-Condon and the transition dipole moment surface levels of theory. The upper panel represents the relative deviation in intensities in the 10^{-18} – $10^{-24} \text{ cm}/\text{molecule}$ intensity range. The lower panel displays transitions to 40 lowest $J'=1$ energy levels of the \tilde{C}^1B_2 state. Transitions to states with a_1 and b_2 symmetries are distinguished.

observed in the $\tilde{C}^1B_2 \leftarrow \tilde{X}^1A_1$ ro-vibronic spectrum.^{48,90,91} The lower panel in Fig. 3 shows several transitions to “ b_2 ” states. The rotation-vibration interaction feeds such transitions with intensity, which is nonetheless usually of 1–3 orders of magnitude weaker than typical vibrationally allowed transitions. We have found a large number of ro-vibrationally allowed and vibrationally forbidden transitions in our line list, for example, transitions in the $\tilde{X}^1A_1(0, 0, 0) \rightarrow \tilde{C}^1B_2(0, 1, 1)$ and $\tilde{X}^1A_1(0, 0, 0) \rightarrow \tilde{C}^1B_2(0, 0, 3)$ manifold. Intensity calculations with Coriolis-decoupled wavefunctions do not reveal any vibrationally forbidden transitions, thereby proving that the rotational-vibrational coupling is responsible for softening of the selection rules for transitions to b_2 states in the \tilde{C}^1B_2 electronic state. The strongest transition to a b_2 state $\tilde{X}^1A_1(0, 0, 0) \rightarrow \tilde{C}^1B_2(0, 1, 3)$ has comparable intensity to many moderately weak vibrationally allowed transitions. In this particular case, the large intensity borrowing can be rationalized by strong Coriolis interaction between the $(0, 1, 3)$ states of b_2 symmetry and the $(0, 0, 4)$ states of a_1 symmetry, which are only separated by 12 cm^{-1} and this leads to strong mixing. A comprehensive discussion of Coriolis interaction between ro-vibrational energy levels of the \tilde{C}^1B_2 electronic state was given by Park *et al.*⁴⁸

Comparison of the FC and TDMS spectrum with semi-empirical FC calculations of Yamanouchi *et al.*⁵⁰ is given in Fig. 4. The assumption of marginal difference between the FC and TDMS spectra is further confirmed in the upper panel in Fig. 4. Line positions in the lower panel correspond to measured values. The agreement between the present study and semi-empirical calculations is satisfying. As previously asserted, the contribution from the TDMS to the spectrum is negligible in this spectral region. Thus for qualitative UV spectrum modeling purposes, the Franck-Condon approximation is sufficient. For higher accuracy, which is required, for example, by remote sensing experiments, the full transition dipole moment surface may be necessary.

Figure 5 gives a comparison between experimental laser-induced fluorescence spectrum by Yamanouchi *et al.*⁵⁰ (upper panel), semi-empirical Franck-Condon vibronic spectra calculated by Xie *et al.*⁶⁶ (middle panel), and present Franck-Condon and TDMS calculations (lowest panel). The overall agreement between the two theoretical studies in the middle and lowest panels is good, with relative intensities following a similar pattern. Changes in intensity caused by the breakdown of the *Condon* approximation are small in this spectral region. In contrast to emission, the initial wavefunction for room-temperature absorption is well localized around the equilibrium geometry of the vibronic ground state, which suppresses transitions to states with largely distorted geometries (cf. Fig. 2). In the 225 nm–235 nm range, line positions and intensities agree well between the present theory and experiment. This agreement however becomes worse for shorter wavelengths. Therefore, below 225 nm, the present \tilde{C}^1B_2 state PES is not accurate enough even for qualitative studies.

Based on the new PES and TDMS, a room temperature (295 K) UV line list for the $\tilde{X}^1A_1 \rightarrow \tilde{C}^1B_2$ electronic transition was calculated in the $J=0$ –40 range. The partition function for the electronic ground state was taken from Huang *et al.*⁸⁴ This line list is designed for the 225 nm–235 nm wavelength range, where it can be considered reliable. A qualitative comparison of the present line list with low-resolution measurements by Wu *et al.*⁹² is given in Fig. 6. Dashed lines

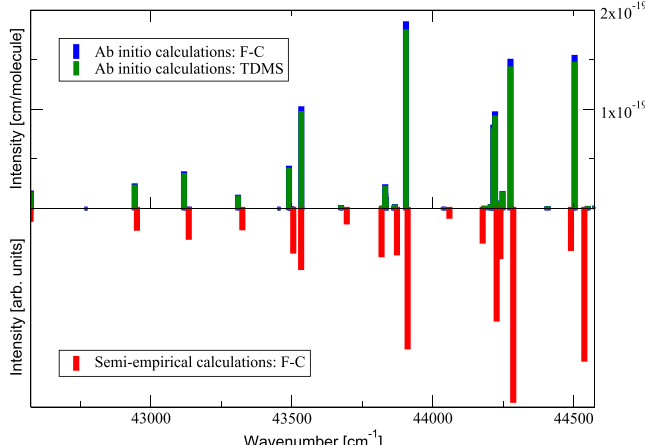


FIG. 4. Comparison of three calculated vibronic spectra: semi-empirical calculations from Yamanouchi *et al.*⁵⁰ in the lower panel; FC and TDMS *ab initio* calculations from the present study in the upper panel. Line positions are given in the 42 500–44 500 cm⁻¹ range.

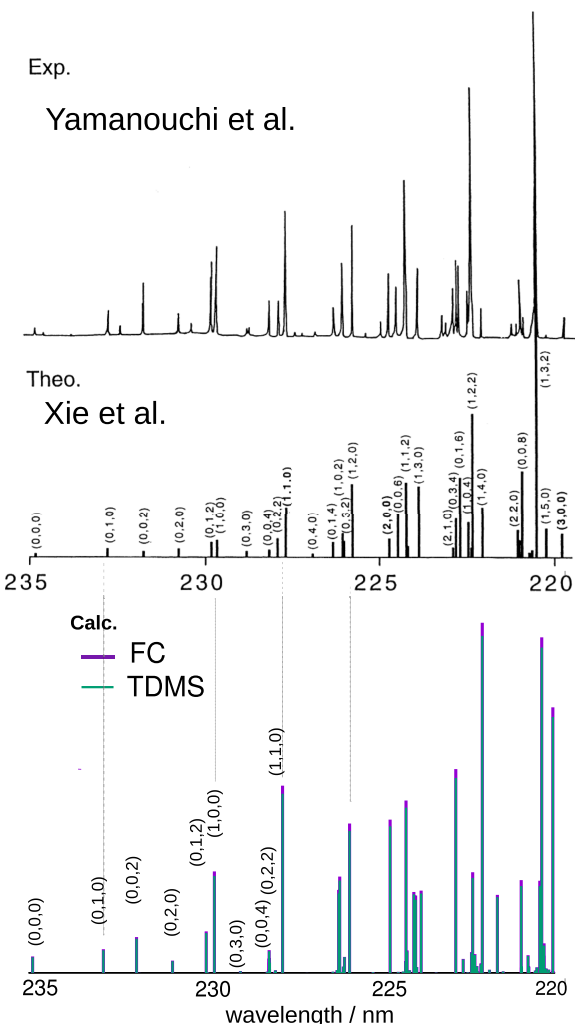


FIG. 5. Comparison of calculated vibronic spectra with measurement by Yamanouchi *et al.*⁵⁰ and semi-empirical calculations of Xie *et al.*⁶⁶ Vibrational assignments were given for 10 lowest calculated transitions. These transitions can be considered as modeled reliably with the present PES and TDMS. The experimental and theoretical spectra were reprinted with permission from Xie *et al.*, Chem. Phys. Lett. **329**, 503–510 (2000). Copyright 2000 Elsevier.

correspond to the experimental cross section (in cm²) measured at 295 K with 0.5 Å resolution. *Ab initio* absorption cross sections are marked in red and green in Fig. 6 and were obtained from integral line intensities by convolution with the Gaussian profile function with full-width at half-maximum (FWHM) of 0.3 cm⁻¹ and 8 cm⁻¹, respectively; no scaling of line intensities or line positions was made.

The low-resolution theoretical cross section depicted by a green thick line in Fig. 6 qualitatively reproduces the band centers measured by Wu *et al.* Comparison of line intensities is however less straightforward due to the non-uniform base line in the measurements. Hot bands, assigned by Wu *et al.*,⁹² are also visible in the *ab initio* spectrum, as expected. Qualitatively, the calculated spectrum reproduces the features of the measured spectrum; however, for a more detailed insight, the accuracy of the present model should be tested on higher resolution experimental data.

High-resolution measurements of the $\tilde{X}^1A_1 \rightarrow \tilde{C}^1B_2$ electronic band were reported by Rufus *et al.*⁶² (at 295 K) and Blackie *et al.*⁶³ (at 198 K). Cross sections from Blackie

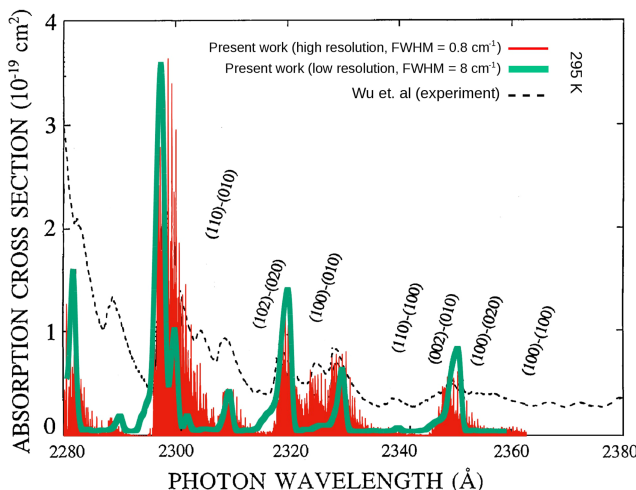


FIG. 6. Comparison of the *ab initio* and measured absorption cross sections. The *ab initio* cross sections were calculated from the room temperature (295 K) ro-vibronic line list for the $\tilde{X}^1A_1 \rightarrow \tilde{C}^1B_2$ electronic transition in SO_2 in the $J=0-40$ range. Gaussian line shapes were used with FWHM of 0.3 cm^{-1} (red thin stick spectrum) and 8 cm^{-1} (green thick line spectrum). Measurements were made by Wu *et al.*⁹² at 295 K. The experimental spectrum was reprinted with permission from Wu *et al.*, Icarus **145**, 289–296 (2001). Copyright 2001 Elsevier.

*et al.*⁶³ are compared with cross sections calculated at 198 K from the present *ab initio* line list in Fig. 7. The FWHM of the experimental rotationally resolved cross sections was 0.3 cm^{-1} . In calculations, the Gaussian line shape profile with FWHM = 0.3 cm^{-1} was used and the partition function at 198 K (3246.3) was calculated from ro-vibrational energy levels available from the work of Underwood *et al.*⁴⁴ The shape of the cross section spectrum is nearly insensitive to the addition of transitions with $J > 40$; thus no higher J energy levels need to be calculated for the present comparison. Nonetheless, it is technically possible to obtain a line list with $J > 100$, with the present implementation of the DVR3DUV code.

The uncertainty of the cross sections measured by Blackie *et al.* was estimated 9%–15% for the strongest bands

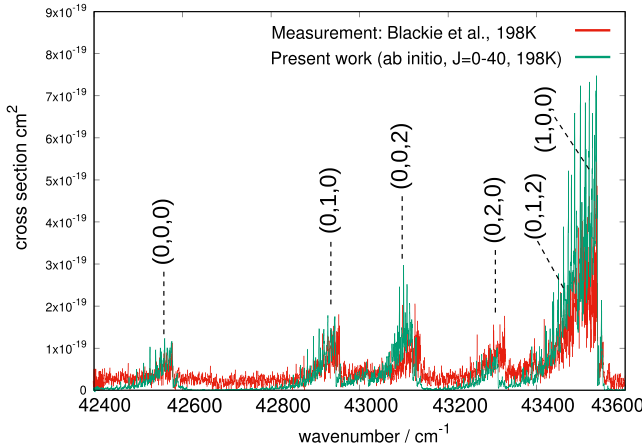


FIG. 7. Comparison of the *ab initio* and measured absorption cross sections. The *ab initio* cross sections were calculated at 198 K from the ro-vibronic line list for the $\tilde{X}^1A_1 \rightarrow \tilde{C}^1B_2$ electronic transition of SO_2 in the $J=0-40$ range. Measurements were made by Blackie *et al.*⁶³ at 198 K. Our vibrational assignments of the spectrum are indicated by dashed lines. All marked transitions are from the vibronic ground state to vibrational states of \tilde{C}^1B_2 .

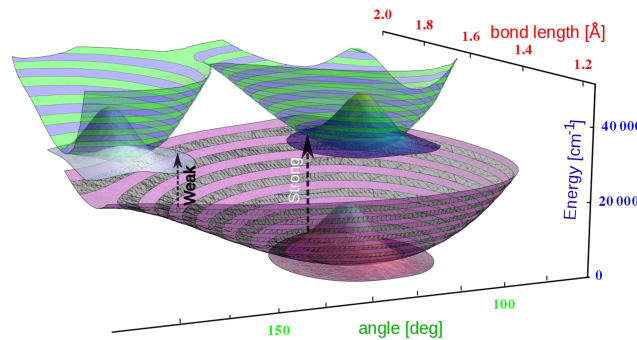


FIG. 8. Potential energy surfaces for \tilde{X}^1A_1 electronic state (purple/grey) and \tilde{C}^1B_2 electronic state (green/blue) of SO_2 . The other bond length is fixed at $r_2 = 1.7 \text{ \AA}$. Wavefunctions for the vibrational ground state of each well are added, with arrows marking Franck-Condon vertical transitions from the electronic ground state.

$\sigma \in (10^{-17} \text{ cm}^2, 10^{-18} \text{ cm}^2)$ and more than 20% for bands weaker than 10^{-18} cm^2 . Overall agreement between the unassigned measured cross sections in Fig. 7 and theoretical cross sections is very good though. Vibronic assignments are also given in Fig. 7. These assignments agree with experimental assignments of Danielache *et al.*⁶⁴ Unfortunately, no ro-vibronic assignments for the experimental spectrum are available, which makes a line by line comparison difficult. A major reason for which the spectrum measured by Blackie *et al.* cannot be presently assigned in the rotational resolution is $10-20 \text{ cm}^{-1}$ uncertainty in *ab initio* line positions. Future studies should focus on obtaining a higher quality, more global PES for the \tilde{C}^1B_2 state. Then, with the use of the present procedure, a purely *ab initio* based ro-vibronic assignment of experimental spectra could become possible.

B. Franck-Condon intensities for a large geometry displacement

The wavefunction for the vibrational ground state in the electronic ground state \tilde{X}^1A_1 of SO_2 is very compact, and most of its amplitude is localized near the C_{2v} equilibrium geometry $r_1^{eq} = 1.431 \text{ \AA}$, $r_2^{eq} = 1.431 \text{ \AA}$, and $\theta^{eq} = 119.32^\circ$, as displayed in Fig. 8. For this reason, the wavefunction overlap between the vibrational ground state of \tilde{X}^1A_1 and vibrational states localized in the second well near $\theta = 165^\circ$ is likely to be very small. Indeed, Table II shows that calculated overlap integrals for transitions to the second well are 4–8 orders

TABLE II. Comparison of vibrational overlap integrals calculated between $J=0$ wavefunctions of the vibronic ground state and vibrational states of the \tilde{C}^1B_2 state. Given in columns are, respectively, ID of the vibrational state belonging to the electronic excited state, overlap integral calculated for the 1st well located at $\theta = 104^\circ$, overlap integral calculated for the 2nd well located at $\theta = 165^\circ$.

State ID	Overlap integral (1st well)	Overlap integral (2nd well)
1	8.48×10^{-3}	2.92×10^{-10}
2	1.41×10^{-2}	1.12×10^{-10}
3	1.73×10^{-2}	-1.41×10^{-11}
4	-2.28×10^{-2}	-2.14×10^{-9}
5	1.67×10^{-4}	-1.84×10^{-9}
6	1.71×10^{-2}	1.12×10^{-9}

of magnitude smaller than the respective factors to the main well, where the global minimum for the \tilde{C}^1B_2 state is located.

It is thus justified to neglect the second well completely in the theoretical intensity calculations. This conclusion is expected to be, in general, applicable to other molecules and other electronic states.

VI. CONCLUSION

In the present work, we report a procedure for calculation of ro-vibronic transition intensities for triatomic molecules. The theoretical scheme is based on accurate calculations of ro-vibrational energy levels and wavefunctions for isolated electronic states in the Born-Oppenheimer approximation, followed by ro-vibronic transition intensity calculations between two electronic states. The scheme presented here gives absolute integral intensities thus is advantageous to traditional approaches based on the Franck-Condon approximation, for which only relative intensities are theoretically available. Rotation-vibration coupled wavefunctions used in the present paper render calculated intensities as inherently more accurate than the standard vibrational Franck-Condon calculations. Inclusion of the transition dipole moment surface alternates intensities of the strongest bands by less than 10% hence may be considered only in quantitative studies. The accuracy of calculated transition intensities depends strongly on the quality of potential energy surfaces, especially for the electronic excited state, for which many vibrational states are required, and which is normally more challenging to generate. This aspect is particularly important for atmospheric science. For example, in the case of SO_2 , the high resolution modeling of the strongest absorption region associated with the $\tilde{C}^1B_2 \leftarrow \tilde{X}^1A_1$ electronic transition is still troublesome with the model presented here. However, this is solely because the location of the strongest absorption in this band near $50\,000\,\text{cm}^{-1}$ requires the calculation of highly excited ro-vibrational states of the \tilde{C}^1B_2 electronic state, and for this reason an accurate and global PES for this state is needed. With high quality potential energy surfaces provided, the theoretical framework presented in this work can be readily applied to other ro-vibronic bands of SO_2 and other molecules, such as ozone.

An aspect of the ro-vibronic problem which we do not address is extending beyond the single state approximation. As shown by Yurchenko and co-workers for diatomic molecules,^{26,93,94} often a significant number of electronic states contribute to the vibronic spectrum; this number is typically larger than three. The computer program DUO due to Yurchenko *et al.*⁹⁵ treats full ro-vibronic calculations, allowing for interaction of an arbitrary number of electronic states in diatomic molecules. A triatomic analogue of DUO is the ultimate aim of the study initiated in this work.

SUPPLEMENTARY MATERIAL

See [supplementary material](#) for Fortran95 routines generating the potential energy surface and the transition dipole moment surface described in Sec. III.

ACKNOWLEDGMENTS

This work is supported by European Research Council project *Exolights*, Award No. 617119. The authors acknowledge the use of the UCL Legion High Performance Computing Facility (Legion@UCL) and associated support services in the completion of this work.

- ¹G. Tinetti, T. Encrenaz, and A. Coustenis, *Astron. Astrophys. Rev.* **21**, 1 (2013).
- ²J. Tennyson and S. N. Yurchenko, *Mol. Astrophys.* **8**, 1 (2017).
- ³I. E. Gordon, L. S. Rothman, Y. Babikov, A. Barbe, D. Chris Benner, P. F. Bernath, M. Birk, L. Bizzocchi, V. Boudon, L. R. Brown, A. Campargue, K. Chance, E. A. Cohen, L. H. Coudert, V. M. Devi, B. J. Drouin, A. Fayt, J.-M. Flaud, R. R. Gamache, J. J. Harrison, J.-M. Hartmann, C. Hill, J. T. Hodges, D. Jacquemart, A. Jolly, J. Lamouroux, R. J. Le Roy, G. Li, D. A. Long, O. M. Lyulin, C. J. Mackie, S. T. Massie, S. Mikhailenko, H. S. P. Müller, O. V. Naumenko, A. V. Nikitin, J. Orphal, V. Perevalov, A. Perrin, E. R. Polovtseva, C. Richard, M. A. H. Smith, E. Starikova, K. Sung, S. Tashkun, J. Tennyson, G. C. Toon, V. G. Tyuterev, G. Wagner, and E. J. Zak, “The HITRAN2016 molecular spectroscopic database,” *J. Quant. Spectrosc. Radiat. Transfer* (in press).
- ⁴L. S. Rothman, I. E. Gordon, R. J. Barber, H. Dothe, R. R. Gamache, A. Goldman, V. I. Perevalov, S. A. Tashkun, and J. Tennyson, *J. Quant. Spectrosc. Radiat. Transfer* **111**, 2139 (2010).
- ⁵N. Jacquinot-Husson, R. Armante, N. A. Scott, A. Chédin, L. Crépeau, C. Boutammine, A. Bouhdaoui, C. Crevoisier, V. Capelle, C. Bonne *et al.*, *J. Mol. Spectrosc.* **327**, 31 (2016).
- ⁶J. Tennyson, M. A. Kostin, P. Barletta, G. J. Harris, O. L. Polyansky, J. Ramamal, and N. F. Zobov, *Comput. Phys. Commun.* **163**, 85 (2004).
- ⁷E. Zak, J. Tennyson, O. L. Polyansky, L. Lodi, S. A. Tashkun, and V. I. Perevalov, *J. Quant. Spectrosc. Radiat. Transfer* **177**, 31 (2016).
- ⁸E. J. Zak, J. Tennyson, O. L. Polyansky, L. Lodi, N. F. Zobov, S. A. Tashkun, and V. I. Perevalov, *J. Quant. Spectrosc. Radiat. Transfer* **189**, 267 (2017).
- ⁹E. J. Zak, J. Tennyson, O. L. Polyansky, L. Lodi, N. F. Zobov, S. A. Tashkun, and V. I. Perevalov, “Room temperature linelists for CO_2 asymmetric isotopologues with ab initio computed intensities,” *J. Quant. Spectrosc. Radiat. Transfer* (in press).
- ¹⁰T. A. Odintsova, E. Faschi, L. Moretti, E. J. Zak, O. L. Polyansky, J. Tennyson, L. Gianfrani, and A. Castrillo, *J. Chem. Phys.* **146**, 244309 (2017).
- ¹¹A. G. Császár, E. Mátyus, L. Lodi, N. F. Zobov, S. V. Shirin, O. L. Polyansky, and J. Tennyson, *J. Quant. Spectrosc. Radiat. Transfer* **111**, 1043 (2010).
- ¹²O. L. Polyansky, N. F. Zobov, I. I. Mizus, L. Lodi, S. N. Yurchenko, J. Tennyson, A. G. Császár, and O. V. Boyarkin, *Philos. Trans. R. Soc., A* **370**, 2728 (2012).
- ¹³J. Tennyson, P. F. Bernath, L. R. Brown, A. Campargue, M. R. Carleer, A. G. Császár, L. Daumont, R. R. Gamache, J. T. Hodges, O. V. Naumenko *et al.*, *J. Quant. Spectrosc. Radiat. Transfer* **117**, 29 (2013).
- ¹⁴L. Birk, G. Wagner, J. Loos, L. Lodi, O. L. Polyansky, A. A. Kyuberis, N. F. Zobov, and J. Tennyson, “Accurate line intensities for water transitions in the infrared: Comparison of theory and experiment,” *J. Quant. Spectrosc. Radiat. Transfer* (in press).
- ¹⁵A. A. Kyuberis, N. F. Zobov, O. V. Naumenko, B. A. Voronin, O. L. Polyansky, L. Lodi, A. Liu, S.-M. Hu, and J. Tennyson, “Room temperature line lists for deuterated water,” *J. Quant. Spectrosc. Radiat. Transfer* (in press).
- ¹⁶T. Sako and K. Yamanouchi, *Chem. Phys. Lett.* **264**, 403 (1997).
- ¹⁷O. N. Ulenikov, E. S. Bekhtereva, V.-M. Horneman, S. Alanko, and O. V. Gromova, *J. Mol. Spectrosc.* **255**, 111 (2009).
- ¹⁸O. N. Ulenikov, G. A. Onopenko, O. V. Gromova, E. S. Bekhtereva, and V.-M. Horneman, *J. Quant. Spectrosc. Radiat. Transfer* **130**, 220 (2013).
- ¹⁹J. Tennyson, *J. Mol. Spectrosc.* **298**, 1 (2014).
- ²⁰J. Jiang, G. B. Park, and R. W. Field, *J. Chem. Phys.* **144**, 144312 (2016).
- ²¹S. Tashkun, V. Perevalov, J.-L. Teffo, M. Lecoutre, T. Huet, A. Campargue, D. Bailly, and M. Esplin, *J. Mol. Spectrosc.* **200**, 162 (2000).
- ²²B. V. Perevalov, A. Campargue, B. Gao, S. Kassi, S. A. Tashkun, and V. I. Perevalov, *J. Mol. Spectrosc.* **252**, 190 (2008).
- ²³K. F. Song, S. Kassi, S. A. Tashkun, V. I. Perevalov, and A. Campargue, *J. Quant. Spectrosc. Radiat. Transfer* **111**, 332 (2010).
- ²⁴X. Huang, D. W. Schwenke, R. S. Freedman, and T. J. Lee, “Ames-2016 line lists for 13 isotopologues of CO_2 : Updates, consistency, and remaining issues,” *J. Quant. Spectrosc. Radiat. Transfer* (in press).
- ²⁵C. Sousa-Silva, S. N. Yurchenko, and J. Tennyson, *J. Mol. Spectrosc.* **288**, 28 (2013).

- ²⁶L. K. McKemmish, S. N. Yurchenko, and J. Tennyson, *Mon. Not. R. Astron. Soc.* **463**, 771 (2016).
- ²⁷A. I. Pavlyuchko, S. N. Yurchenko, and J. Tennyson, *Mon. Not. R. Astron. Soc.* **452**, 1702 (2015).
- ²⁸T. E. Odaka, T. Hirano, and P. Jensen, *J. Mol. Spectrosc.* **211**, 147 (2002).
- ²⁹T. E. Odaka, V. V. Melnikov, P. Jensen, T. Hirano, B. Lang, and P. Langer, *J. Chem. Phys.* **126**, 094301 (2007).
- ³⁰V. V. Melnikov, T. E. Odaka, P. Jensen, and T. Hirano, *J. Chem. Phys.* **128**, 114316 (2008).
- ³¹P. Jensen, M. Brumm, W. Kraemer, and P. Bunker, *J. Mol. Spectrosc.* **171**, 31 (1995).
- ³²T. Hirano, V. Derpmann, U. Nagashima, and P. Jensen, *J. Mol. Spectrosc.* **263**, 150 (2010).
- ³³I. F. C. Mbapeh, S. C. G. Kempf, and P. Jensen, *J. Phys. Chem. A* **119**, 10112 (2015).
- ³⁴B. Ostojić, P. Jensen, P. Schwerdtfeger, and P. R. Bunker, *J. Phys. Chem. A* **117**, 9370 (2013).
- ³⁵S. Carter, N. C. Handy, C. Puzzarini, R. Tarroni, and P. Palmieri, *Mol. Phys.* **98**, 1697 (2000).
- ³⁶T. Taketsugu, K. Ishii, and S. Carter, *Chem. Phys. Lett.* **380**, 213 (2003).
- ³⁷S. Carter, N. C. Handy, and R. Tarroni, *Mol. Phys.* **103**, 1131 (2005).
- ³⁸Z. Bacic and J. C. Light, *Annu. Rev. Phys. Chem.* **40**, 469 (1989).
- ³⁹J. C. Light and T. Carrington, *Adv. Chem. Phys.* **114**, 263 (2000).
- ⁴⁰X.-G. Wang and T. Carrington, Jr., *J. Chem. Phys.* **130**, 094101 (2009).
- ⁴¹J. Tennyson and S. N. Yurchenko, *Int. J. Quantum Chem.* **117**, 92 (2017).
- ⁴²J. Tennyson and B. T. Sutcliffe, *Mol. Phys.* **58**, 1067 (1986).
- ⁴³L. Lodi and J. Tennyson, *J. Quant. Spectrosc. Radiat. Transfer* **113**, 850 (2012).
- ⁴⁴D. S. Underwood, J. Tennyson, S. N. Yurchenko, X. Huang, D. W. Schwenke, T. J. Lee, S. Clausen, and A. Fateev, *Mon. Not. R. Astron. Soc.* **459**, 3890 (2016).
- ⁴⁵O. L. Polyansky, K. Bielska, M. Ghysels, L. Lodi, N. F. Zobov, J. T. Hodges, and J. Tennyson, *Phys. Rev. Lett.* **114**, 243001 (2015).
- ⁴⁶Q. Meng and H.-D. Meyer, *J. Chem. Phys.* **141**, 124309 (2014).
- ⁴⁷T. J. Penfold and G. A. Worth, *J. Mol. Graphics Modell.* **26**, 613 (2007).
- ⁴⁸G. B. Park, J. Jiang, C. A. Saladrigas, and R. W. Field, *J. Chem. Phys.* **144**, 144311 (2016).
- ⁴⁹C. G. Parigger and J. O. Hornkohl, *Spectrochim. Acta, Part A* **81**, 404 (2011).
- ⁵⁰K. Yamamotochi, M. Okunishi, Y. Endo, and S. Tsuchiya, *J. Mol. Struct.* **352-353**, 541 (1995).
- ⁵¹T. Hirano and U. Nagashima, *J. Mol. Spectrosc.* **314**, 35 (2015).
- ⁵²H. Mustroph, *Comput. Phys. Commun.* **17**, 2616 (2016).
- ⁵³A. R. Whitehill, C. Xie, X. Hu, D. Xie, H. Guo, and S. Ono, *Proc. Natl. Acad. Sci. U. S. A.* **110**, 17697 (2013).
- ⁵⁴C. R. Nowlan, X. Liu, K. Chance, Z. Cai, T. P. Kurosu, C. Lee, and R. V. Martin, *J. Geophys. Res.* **116**, D18301, doi:10.1029/2011jd015808 (2011).
- ⁵⁵N. Krotkov, S. Carn, A. Krueger, P. Bhartia, and K. Yang, *IEEE Trans. Geosci. Electron.* **44**, 1259 (2006).
- ⁵⁶N. Theys, R. Campion, L. Clarisse, H. Brenot, J. van Gent, B. Dilis, S. Corradini, L. Merucci, P.-F. Coheur, M. V. Roozendael *et al.*, *Atmos. Chem. Phys.* **13**, 5945 (2013).
- ⁵⁷E. Klisch, P. Schilke, S. Belov, and G. Winnewisser, *J. Mol. Spectrosc.* **186**, 314 (1997).
- ⁵⁸L. M. Ziurys, *Proc. Natl. Acad. Sci. U. S. A.* **103**, 12274 (2006).
- ⁵⁹C. Xie, X. Hu, L. Zhou, D. Xie, and H. Guo, *J. Chem. Phys.* **139**, 014305 (2013).
- ⁶⁰G. B. Park, J. Jiang, and R. W. Field, *J. Chem. Phys.* **144**, 144313 (2016).
- ⁶¹D. E. Freeman, K. Yoshino, J. R. Esmond, and W. H. Parkinson, *Planet. Space Sci.* **32**, 1125 (1984).
- ⁶²J. Rufus, G. Stark, P. L. Smith, J. C. Pickering, and A. P. Thorne, *J. Geophys. Res.: Planets* **108**, 5011, doi:10.1029/2002je001931 (2003).
- ⁶³D. Blackie, R. Blackwell-Whitehead, G. Stark, J. C. Pickering, P. L. Smith, J. Rufus, and A. P. Thorne, *J. Geophys. Res.* **116**, E03006, doi:10.1029/2011je003977 (2011).
- ⁶⁴S. O. Danielache, C. Eskebjerg, M. S. Johnson, Y. Ueno, and N. Yoshida, *J. Geophys. Res.* **113**, D17314, doi:10.1029/2007jd009695 (2008).
- ⁶⁵T. Sako, A. Hishikawa, and K. Yamanouchi, *Chem. Phys. Lett.* **294**, 571 (1998).
- ⁶⁶D. Xie, H. Guo, O. Bludsky, and P. Nachtigall, *Chem. Phys. Lett.* **329**, 503 (2000).
- ⁶⁷O. Bludský, P. Nachtigall, J. Hrušák, and P. Jensen, *Chem. Phys. Lett.* **318**, 607 (2000).
- ⁶⁸J. Klos, M. H. Alexander, P. Kumar, B. Poirier, B. Jiang, and H. Guo, *J. Chem. Phys.* **144**, 174301 (2016).
- ⁶⁹P. Kumar, B. Jiang, H. Guo, J. Klos, M. H. Alexander, and B. Poirier, *J. Phys. Chem. A* **121**, 1012 (2017).
- ⁷⁰J. T. Hougen and J. K. G. Watson, *Can. J. Phys.* **43**, 298 (1965).
- ⁷¹D. M. Jonas, X. Yang, and A. M. Wodtke, *J. Chem. Phys.* **97**, 2284 (1992).
- ⁷²G. M. Sando and K. G. Spears, *J. Phys. Chem. A* **105**, 5326 (2001).
- ⁷³P. Meier and G. Rauhut, *Mol. Phys.* **113**, 3859 (2015).
- ⁷⁴D. L. Kokkin, T. Ma, T. Steimle, and T. J. Sears, *J. Chem. Phys.* **144**, 244304 (2016).
- ⁷⁵P. R. Bunker and P. Jensen, *Molecular Symmetry and Spectroscopy*, 2nd ed. (NRC Research Press, Ottawa, Canada, 2006), ISBN: 0-660-17519-3.
- ⁷⁶J. Tennyson and B. T. Sutcliffe, *Int. J. Quantum Chem.* **42**, 941 (1992).
- ⁷⁷B. R. Johnson and W. P. Reinhardt, *J. Chem. Phys.* **85**, 4538 (1986).
- ⁷⁸B. T. Sutcliffe and J. Tennyson, *Int. J. Quantum Chem.* **39**, 183 (1991).
- ⁷⁹J. Tennyson, *Comput. Phys. Commun.* **42**, 257 (1986).
- ⁸⁰B. T. Sutcliffe, S. Miller, and J. Tennyson, *Comput. Phys. Commun.* **51**, 73 (1988).
- ⁸¹F.-T. Chau, J. M. Dyke, E. P. F. Lee, and D. K. W. Mok, *J. Chem. Phys.* **115**, 5816 (2001).
- ⁸²X. Yang, C. A. Rogaski, and A. M. Wodtke, *J. Opt. Soc. Am. B* **7**, 1835 (1990).
- ⁸³H.-J. Werner, P. J. Knowles, G. Knizia, F. R. Manby, and M. Schütz, *Wiley Interdiscip. Rev.: Comput. Mol. Sci.* **2**, 242 (2012).
- ⁸⁴X. Huang, D. W. Schwenke, and T. J. Lee, *J. Chem. Phys.* **140**, 114311 (2014).
- ⁸⁵X. Huang, D. W. Schwenke, and T. J. Lee, *J. Mol. Spectrosc.* **311**, 19 (2016).
- ⁸⁶J. Tennyson and B. T. Sutcliffe, *J. Chem. Phys.* **77**, 4061 (1982).
- ⁸⁷G. Audi and A. H. Wapstra, *Nucl. Phys. A* **595**, 409 (1995).
- ⁸⁸I. Tokue and S. Nanbu, *J. Chem. Phys.* **132**, 024301 (2010).
- ⁸⁹K. C. Thompson, M. J. T. Jordan, and M. A. Collins, *J. Chem. Phys.* **108**, 8302 (1998).
- ⁹⁰B. Parsons, L. J. Butler, D. Xie, and H. Guo, *Chem. Phys. Lett.* **320**, 499 (2000).
- ⁹¹P. C. Ray, M. F. Arendt, and L. J. Butler, *J. Chem. Phys.* **109**, 5221 (1998).
- ⁹²C. Wu, B. W. Yang, F. Z. Chen, D. L. Judge, J. Caldwell, and L. M. Trafton, *Icarus* **145**, 289 (2000).
- ⁹³L. Lodi, S. N. Yurchenko, and J. Tennyson, *Mol. Phys.* **113**, 1998 (2015).
- ⁹⁴S. N. Yurchenko, A. Blissett, U. Asari, M. Vasilios, C. Hill, and J. Tennyson, *Mon. Not. R. Astron. Soc.* **456**, 4524 (2016).
- ⁹⁵S. N. Yurchenko, L. Lodi, J. Tennyson, and A. V. Stolyarov, *Comput. Phys. Commun.* **202**, 262 (2016).